Trans Indian Inst Met (2018) 71(6):1519–1529
https://doi.org/10.1007/s12666-018-1287-y

TECHNICAL PAPER

Microstructure, Mechanical and Sliding Wear Behavior of AA5083–B_4C/SiC/TiC Surface Composites Fabricated Using Friction Stir Processing

Vikram Kumar S. Jain[1] · P. M. Muhammed[1] · S. Muthukumaran[1] · S. P. Kumaresh Babu[1]

Received: 4 August 2017 / Accepted: 30 January 2018 / Published online: 24 February 2018

Abstract In this research, friction stir processing (FSP) was used to produce three different surface composites of AA5083 reinforced with B_4C, SiC, and TiC particles. The effects of reinforced particles and three consecutive FSP passes on particle distribution, microstructure, mechanical and wear properties were studied. The microstructure reveals significant grain refinement with a dense distribution of particulates towards the retreating side and advancing side of stir zone, some region at the centre of stir zone shows particle free bands and excellent bonding between particle and matrix. FSP induces severe plastic deformation promoting mixing and refining the constituent phase in the materials. Mechanical properties and wear resistance of the FSPed samples were evaluated and compared with the matrix alloy. The results show that the incorporation of B_4C, SiC and TiC particles into the matrix improves the hardness, tensile and wear properties. TiC and SiC particulates reinforced surface composites reveals a ductile mode of fracture whereas B_4C reinforced surface composite shows a bimodal type of fracture. The investigation on wear mechanism was performed using a pin-on-disc tribometer. The results show that the wear mode changes from abrasive to delamination wear.

Keywords Friction stir processing · AA5083 · Characterization · Mechanical properties · Wear resistance

✉ S. Muthukumaran
smuthu@nitt.edu

Vikram Kumar S. Jain
vkjainpesit@gmail.com

[1] Department of Metallurgical and Materials Engineering, National Institute of Technology, Tiruchirappalli, Tiruchirappalli, Tamil Nadu 620 015, India

1 Introduction

Aluminum reinforced with different particulates exhibit a unique combination of mechanical and tribological properties, which finds potential applications in automotive, aerospace, transport, shipbuilding industries and defence sector [1]. The fabrication of bulk metal matrix composites by conventional and powder metallurgy route exhibits several drawbacks which include inhomogeneous distribution (agglomeration) of the reinforced particles, the interfacial reaction between the particle and matrix, and segregation of particles along grain boundary which lower the performance of composites. These composites fabricated via conventional methods show poor ductility and toughness [2–6]. The in situ fabrication technique is the ideal one, which displays better metallurgical microstructure and mechanical properties because of excellent bonding of particles with the matrix, clean particle–matrix interface. Friction stir processing (FSP) is a new solid-state technique used to modify the surface, mechanical and microstructure features of metallic materials [7]. For many engineering applications, the service life of the component often depends upon their surface properties such as wear resistance. Therefore surface composites fabricated via friction stir processing leads to enhance the surface properties counter the wear and mechanical properties [8–12]. The principle behind FSP is friction stir welding (FSW) process. During FSP, the non-consumable rotating tool with a pin and shoulder is plunged into a workpiece and traverses along the processing direction. The friction between the workpiece and tool generates heat and softens the workpiece. The combined effect of tool and traverse speed induces plastic deformation, and dynamic mixing of materials resulting in uniform dispersion of particles. Mahmoud et al. [13] studied the feasibility of surface

composite by dispersion of SiC particles in the aluminum matrix. Shafiei-zarghani et al. [14] produced Al6082/Al_2O_3 composite by FSP subjected to 1–4 passes. After the 4th pass, Al6082/Al_2O_3 composite shows an improvement in hardness, strength, distribution of particles and wear resistance. Rejil et al. [15] fabricated hybrid surface composite layer (AA 6360–B4C–TiC) by varying volume fraction of particulate and reported that in combined form, hybrid surface composite shows higher wear resistance. Soleymani et al. [16] manufactured AA5083–SiC–MoS_2 hybrid surface composite layer. The SiC particles in the AA5083 matrix improves the hardness and wear resistance. The MoS_2 particles promote lubrication effect. Therefore wear properties are enhanced. Yuvaraj et al. [17] studied wear behavior of mono and hybrid nanocomposite by FSP. The multiple FSP passes are preferred for better dispersion of particulates in an aluminum matrix. Literature survey shows that FSP has been successfully carried out to fabricate aluminum metal matrix composites with various reinforcement including TiC, B4C, SiC, Si_3N_4, TiO_2, TiN, Al_2O_3, ZrO_2, BN, CeO_2, and CNT's. However, no information exists as regards the study of different particulates reinforced with AA5083 alloy with identical experimental parametric conditions. In the present work, aluminum 5083 alloy has been reinforced with three different particulates to fabricate surface composite via FSP. Among the various reinforcements, B4C, SiC, and TiC have attracted much attention due to their superior mechanical and physical properties reported elsewhere [18–20]. The rotating speed of 1600 rpm, the transverse speed of 25 mm/min, tool tilt angle of 3° and multiple passes were selected based on experimental trails to produce sound FSP region and homogeneous dispersion of particulates in the stirred zone. The effect of various particulates on microstructure, mechanical and tribological properties were investigated.

2 Experimental Procedure

A 6 mm thick AA5083 aluminum alloy plate with a nominal chemical composition is listed in Table 1.

The samples were prepared from the AA5083 alloy plates to the dimension of 150 × 80 × 6 mm^3. The three different particulates such as B_4C (99.5% and particle size of 3 μm), SiC (99% and particle size of 8 μm), and TiC (99% purity and particle size of 5 μm) were selected as reinforcements. The SEM micrographs of particulates are shown in Fig. 1. A groove of 1 mm width and 2.5 mm depth was machined on the plate to incorporate particulates. The top surface of the groove was closed using pinless tool with a rotational speed of 800 rpm and traverse speed of 40 mm/min. The tool with a pin was then used to perform FSP with a rotational speed of 1600 rpm, traverse speed of 20 mm/min, the tilt angle of 3° and three passes were carried out to disperse the reinforcements in an AA5083 matrix. The FSP tool has a shoulder diameter of 18 mm, pin length of 4 mm, taper threaded pin with a top diameter of 6 mm and a bottom diameter of 4 mm as shown in the Fig. 2a, b.

Table 1 Chemical compositions of the base alloy AA5083

Elements	Mg	Si	Mn	Cr	Fe	Cu	Zn	Ti	Al
Wt%	4.7	0.2	0.9	0.09	0.7	0.28	0.05	0.05	Bal.

The FSP was carried out on a 4-axis numerically controlled friction stir welding machine (M/s BiSS-ITW, Bengaluru). Figure 3 shows the schematic of friction stir processing. The microstructural studies were carried out on the optical microscope and SEM. The cross-sectioned samples perpendicular to the FSP direction were polished with different grades of SiC papers. The mirror-like finish was obtained using diamond paste on the disc polishing machine as per standard metallographic techniques. Etching was carried out using modified Poulton's reagent to reveal grain boundary. The mean grain size was measured on FSPed samples according to ASTM linear intercept method (ASTM: E112-96).

The microhardness (Matsuzawa MMT-X) was measured on polished samples using an indenter with a 100 g load for 10 s dwell time. Tensile tests of the base alloy and surface composite samples were carried out on Tinius Olsen tensile testing machine at the strain rate of 1 mm/min. The tensile samples were prepared as per ASTM E8/E8 M-11 standards and shown in Fig. 4. The sliding wear test was conducted using a pin on disc tribometer at room temperature as per ASTM G99-05 standards. The samples with a size of 3 mm × 5 mm × 20 mm were machined from the FSPed region using wire EDM. The sliding wear behavior was evaluated using sliding velocity of 1.0 m/s, a load of 20 N and sliding distance of 1000 m.

3 Results and Discussion

3.1 Macro and Microstructural Characterization

Figure 5 shows the cross-sectioned image of the stir zone of three different surface composites. The surface composite specimens appear to be free of defects. This can be attributed to the intense stirring action of the tool which plasticizes material leading to severe plastic deformation. Figure 5a depicts the dense formation of particles towards retreating side (RS) of the AA5083–B_4C surface composite than the advancing side (AS) which may be due to throwing away of the particles by pin during stirring action.

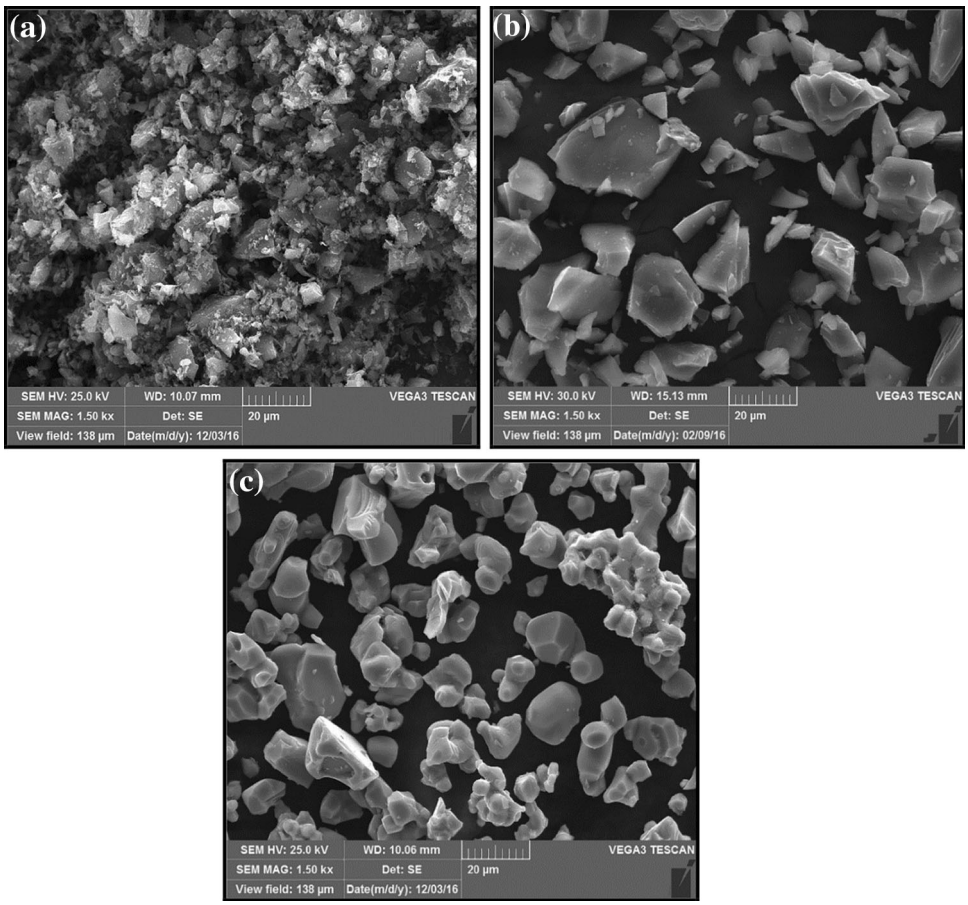

Fig. 1 Micrographs of powder particles of **a** B_4C, **b** SiC, **c** TiC

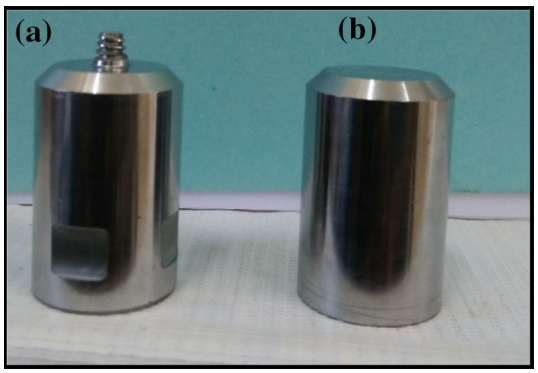

Fig. 2 Friction stir processing tool **a** tapered threaded tool (pin tool). **b** Pin-less tool

The stir zone of AA5083–SiC surface composite reveals the uniform distribution of particles just below the top surface and a particle-free region at the centre of the stir zone. The dense formation of SiC particles is observed at the centre of the RS and AS respectively as shown in Fig. 5b. These difference of free particle regions and dense particles in the matrix is mainly attributed to the material flow phenomenon during FSP. The homogeneous distribution of TiC particles at the stir zone is shown in Fig. 5c.

Figure 6 shows the optical micrographs of different locations of particulates reinforced with AA5083 surface composites, which clearly reveals the dispersion of particulates in the aluminum matrix. It is evident from the micrographs that particulates are clearly visible and no clusters or agglomeration of the particulates are observed. From the micrographs, three zones are distinguished as stirred zone (SZ), thermo-mechanical affected zone (TMAZ) and heat affected zone (HAZ). Recrystallized grains are observed in the stir zone due to severe deformation and heat, resulting in dynamic recrystallization. The TMAZ undergo deformation, but heat required for recrystallized grains are not sufficient. The material flow causes grains to elongate around the revolving pin. The HAZ experience the thermal cycle and does not deform. Figure 6 shows the stir zone of SiC reinforced composite with onion rings structure. The formation of this structure is due to the geometrical effect; materials are extruded and forged from front side to rear side as layer by layer. For homogenous microstructure of surface composites, it is evident from the literature that the combined effect of high rotational speed and transverse speed is not sufficient for distribution and breaking up of a cluster of particles. However, in order to obtain a better dispersion of particulates, a new process

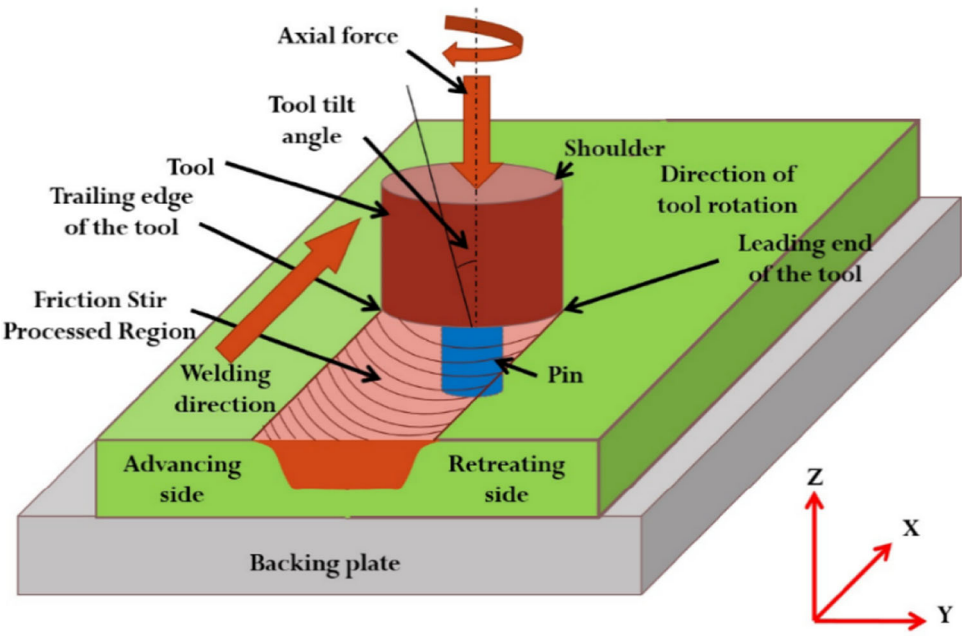

Fig. 3 Schematic drawing of friction stir processing

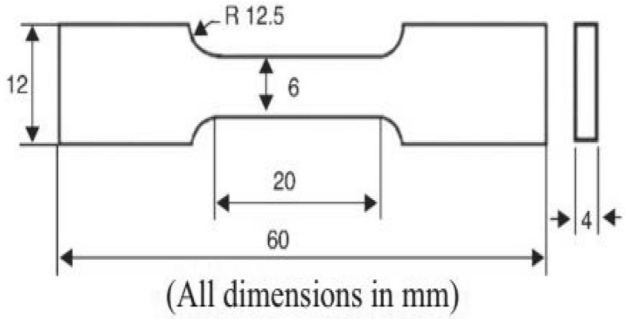

Fig. 4 Schematic sketch of the tensile specimen

parameter has been considered other than aforesaid multiple pass [13, 15, 17]. The cluster of particles is due to the high cohesive energy which in turn increases the surface area and tendency to clump together forming a cluster. The higher hardness of particulates offers resistance during FSP and necessary heat input has not been induced to plasticize the materials which also results in agglomeration or clusters. Therefore higher heat input is desirable in the fabrication of surface composites. Multiple pass sequence has been adopted by several researchers for uniform dispersion of particles [13–15, 21]. The FSP results in the formation of refined grains due to the occurrence of continuous dynamic recrystallization process (CDRX). During the dynamic recrystallization process, fine equiaxed grains are formed due to severe plastic deformation which changes the low angle to high angle grain boundaries. Figure 7 shows the optical images of AA5083 matrix and surface composites. The average grain size of the AA5083 matrix is found to be 42 μm. The embedded B_4C, SiC and TiC particles in the matrix contribute to grain refinement, which acts as heterogeneous nucleation site which further retards the grain growth of matrix. In comparison to the base alloy and after 3 passes of AA5083, surface composites are composed of finer grains. The grain size measurements have been carried out using an image analyzer as per ASTM E112-96 standards and results are tabulated in Table 2.

Some researchers reported the particle segregation which is more vulnerable to mechanical and tribological properties. Segregation of particles is very common in primary processes such as stir casting technique [22–27]. This is attributed to three major phenomena namely buoyant motion of particles, pushing of particles by the moving solidification front and by convention currents in the melts [28]. Moreover, FSP is a solid-state processing, where matrix does not melts. Though there is no occurrence of melting, solidification related problems are absent and density gradient does not cause free movement of particles. This results in uniform dispersion of particulates. The vigorous stirring of tool pin which come in contact with particulates knocks off the sharp corners and form a small fragment of particles whose particle size varies from few microns to nano size. Similar observations were reported by several researcher [8, 13, 15, 29].

3.2 Mechanical Characterization

The variation of microhardness of AA5083 surface composite reinforced with B_4C, SiC and TiC particles are presented in Table 3. The average hardness of the AA5083 alloy is 78 Hv. It is clearly shown that microhardness value for AA5083 surface composite reinforced with B_4C, SiC

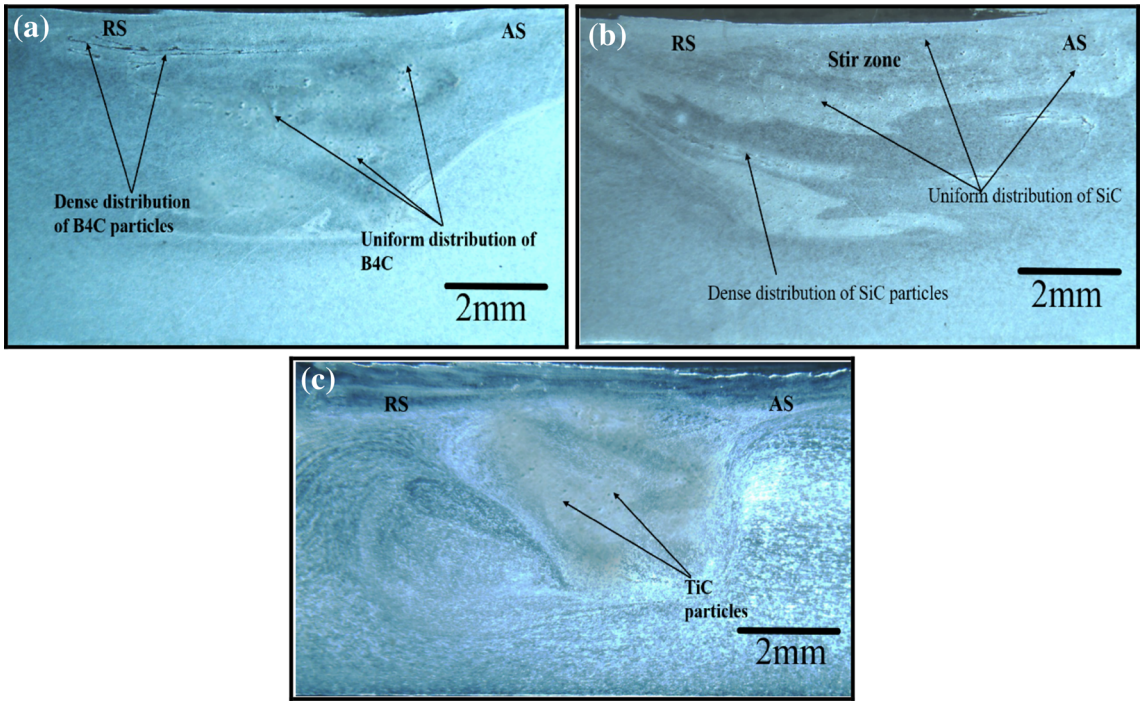

Fig. 5 Cross-sections of the stir zone of **a** B_4C, **b** SiC, **c** TiC reinforced with AA5083

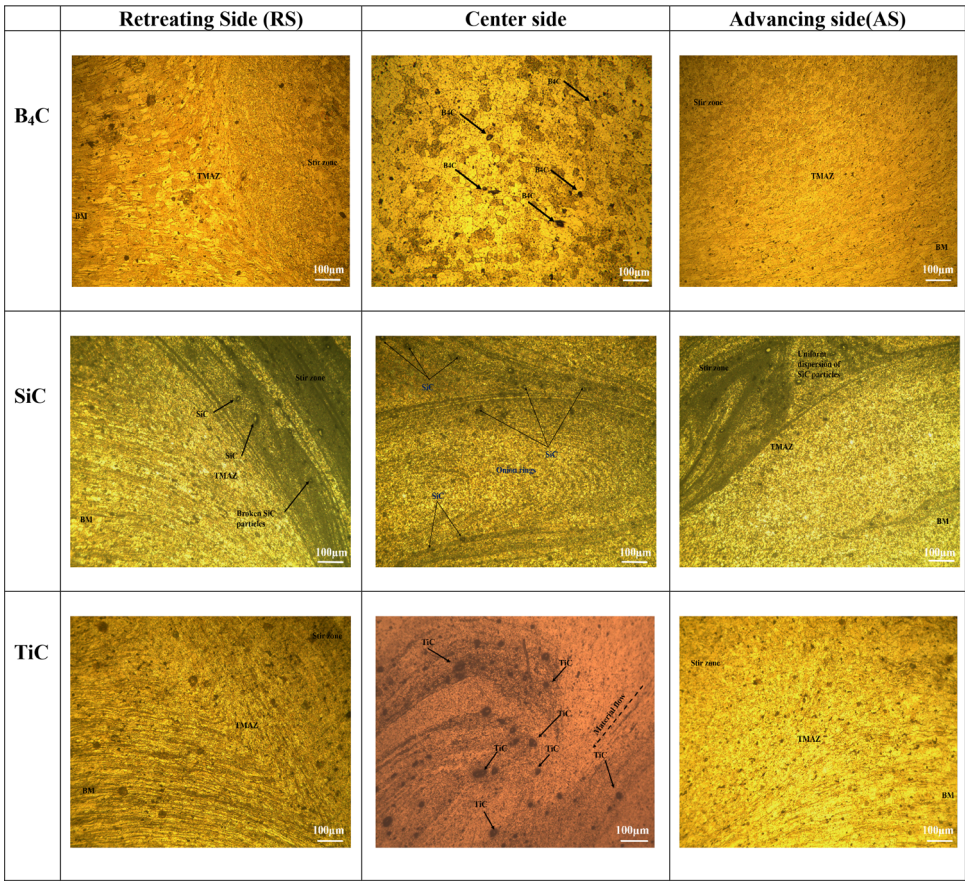

Fig. 6 OM images captured at a different location of surface composite reinforced with B_4C/SiC/TiC microsized particles

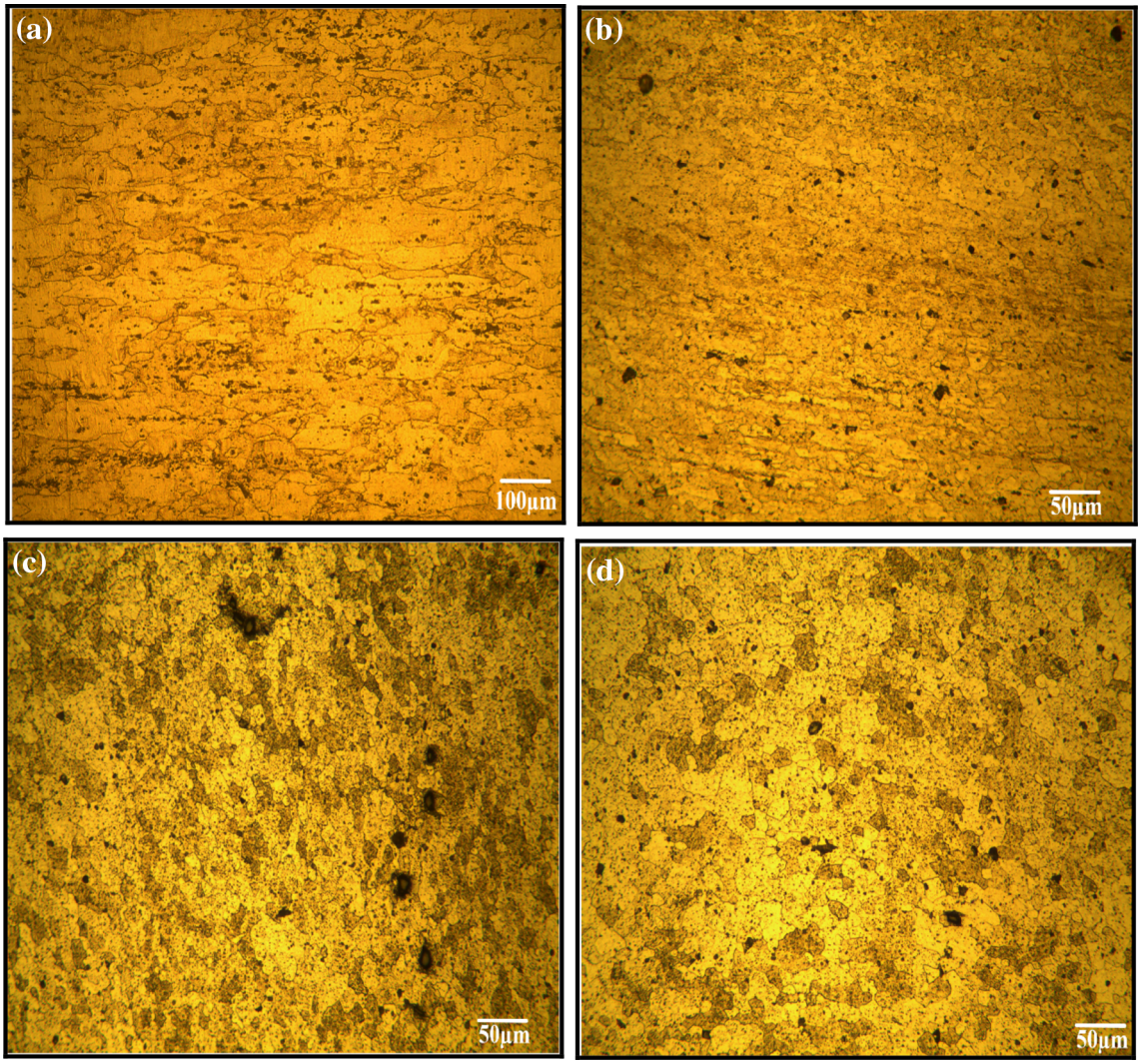

Fig. 7 Optical microstructure of **a** AA5083, and stirred zone microstructure of **b** B_4C, **c** SiC, **d** TiC reinforced surface composites

Table 2 Mean grain size analysis of surface composites

	Grain size (μm)
Base alloy	40.90
AA5083–TiC	5.50
AA5083–SiC	4.90
AA5083–B_4C	3.80

and TiC increases due to the embedded particles and also strengthens the matrix. The strengthening mechanism can be attributed to the following factors such as uniform dispersion of particulates in the stir zone. The uniform distribution of particulates results in pinning effect on the aluminum matrix and retard grain growth and the difference in coefficient of thermal expansion also produces dislocation and consequently, an increase in the hardness can be seen. According to Hall–Petch relationship, it is well known that the grain size influences the mechanical properties. The grain size of the AA5083 surface composite is smaller to that of the aluminum matrix due to the grain refinement owing to dynamic recrystallization process. Furthermore, the homogeneous distribution of particulates in aluminum matrix invokes Orowan strengthening [30]. The maximum hardness of 132.56 ± 2.52 Hv has been obtained for AA5083/B_4C surface composite. However, there is no large differences in the hardness values for other surface composites.

Figure 8 shows the ultimate tensile strength of base alloy and different particulates reinforced with AA5083 surface composite. The ultimate tensile strength of AA5083 surface composite reinforced with B_4C, SiC, TiC and the base alloy is found to be 345, 332, 325 and 298 MPa respectively. During FSP, particulates incorporated in matrix induce dynamic recrystallization and

Table 3 Properties of base alloy and AA5083 surface composites

	Hardness (Hv)	Tensile Strength (MPa)	Elongation (%)	Wear rate ($\times 10^{-5}$ mm^3/Nm)
Base alloy	78.25 ± 1.25	298	26.85	32.85
AA5083–TiC	114.55 ± 1.35	320	18.55	22.28
AA5083–SiC	118.25 ± 1.56	335	13.5	24.25
AA5083–B_4C	132.56 ± 2.52	349	9.25	18.00

pinning effect of particles on matrix retards the grain growth. Furthermore, the addition of particulates induces strength, resistance to tensile stresses resulting in enhanced ultimate strength. The origination of the dislocation density within the grain, subgrain and stacking up of dislocations nearer to grain boundary further enhances mechanical properties. The occurrence of dislocations is due to the difference in coefficient of thermal expansion between the matrix and various particulates. The good bonding and clean interface between particle and matrix play important role in enhancing the tensile properties by transferring the load. Therefore higher stress is essential to initiate the crack between the matrix–particle interfaces resulting in higher tensile strength [31–35]. The addition of particulates drastically reduces the ductility as noticed in the Fig. 8 for the AA5083 surface composite compared to that of base alloy, because of a large amount of stress concentration at the particle–matrix interfaces.

Figure 9a–d shows the SEM fracture image of the tested samples. The base alloy exhibits a ductile failure with larger equiaxed dimples and voids on the fracture surface shown in Fig. 9a. Whereas AA5083 surface composites containing SiC, and TiC particles show smaller dimples and voids in size compared to the base alloy, indicating the ductile mode of fracture. The smaller dimples and voids are attributed to the refinement of grains during dynamic recrystallization and homogeneous dispersion of the particulates in the matrix as shown in Fig. 9b, c. Figure 9d depicts the AA5083–B_4C surface composites exhibiting bimodal type of fracture. The fracture surfaces reveal smaller voids, rough surface and tear ridges which signifies the mixed mode of ductile and brittle fracture. The mechanism involved in the ductile fracture is a large amount of stress concentration nearer to the reinforcing particles that initiate a crack in the particle–matrix interface during the mechanical deformation. The failure occurs due to the associated effects of particle cracking, nucleation, growth and coalescence of microvoids in the matrix. The brittle fracture shows the particle pullouts, de-cohesion of matrix-particles interfaces, crack nucleation and propagation resulting in failure. The surface composites have finer voids and dimples when compared to the matrix, and this is

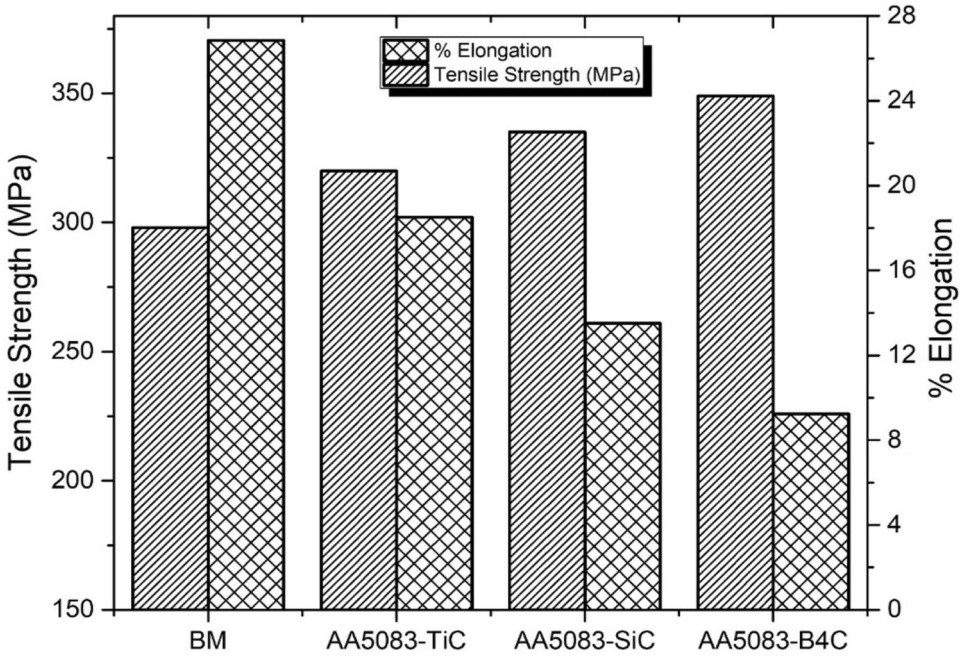

Fig. 8 Ultimate tensile strength and ductility of base alloy and AA5083 surface composites

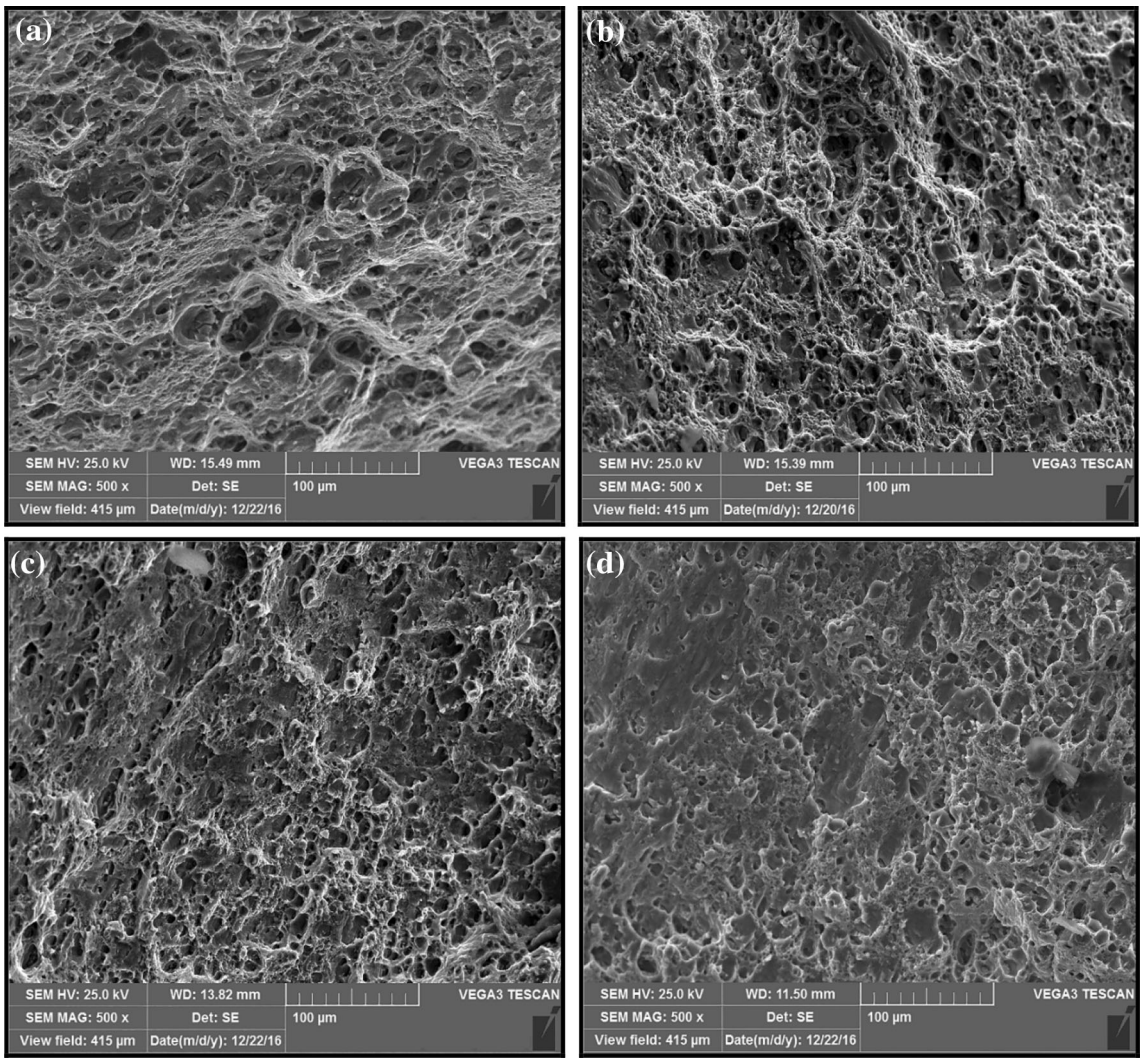

Fig. 9 SEM micrographs of fracture surface of **a** AA5083 alloy, **b** AA5083–TiC, **c** AA5083–SiC, **d** AA5083–B_4C surface composites

due to refined grains of surface composites. Finally, it can be summarized that AA5083, TiC and SiC reinforced surface composites show the ductile mode whereas B_4C reinforced surface composites exhibit the bimodal type of fracture.

3.3 Sliding Wear Behavior of AA5083 Surface Composite

Table 3 shows the variations of the wear rate of the base alloy and AA5083 surface composites. It is clearly observed that AA5083 surface composite in comparison to base alloy, have better wear resistance. The following factors can be attributed to the enhancement of the wear resistance:

1. The uniform dispersion of the particulates induced during the intense stirring action of the tool. As a result of that, fine grain structure and improved hardness are found. According to the Archard wear equation, the wear resistance of materials increases by enhancement of their hardness.
2. Embedded particulates within the matrix have great influence in reducing direct load contact between the matrix and hardened steel disk. Thus reducing the plastic deformation.

Meanwhile, the good interfacial bonding and clean interface of particulates with aluminum matrix by in situ formation may lead to enhancement of properties. Figure 10 displays the SEM micrographs of the worn surface of as received AA5083 and AA5083 surface composite reinforced with different particulates. Figure 10a shows the worn surface of AA5083 alloy resulting in a severe plastic deformation; no excessive damage to the surface is seen along the sliding distance. The long continuous grooves are formed on matrix materials which result in ploughing action and removing or pushing the material into ridges

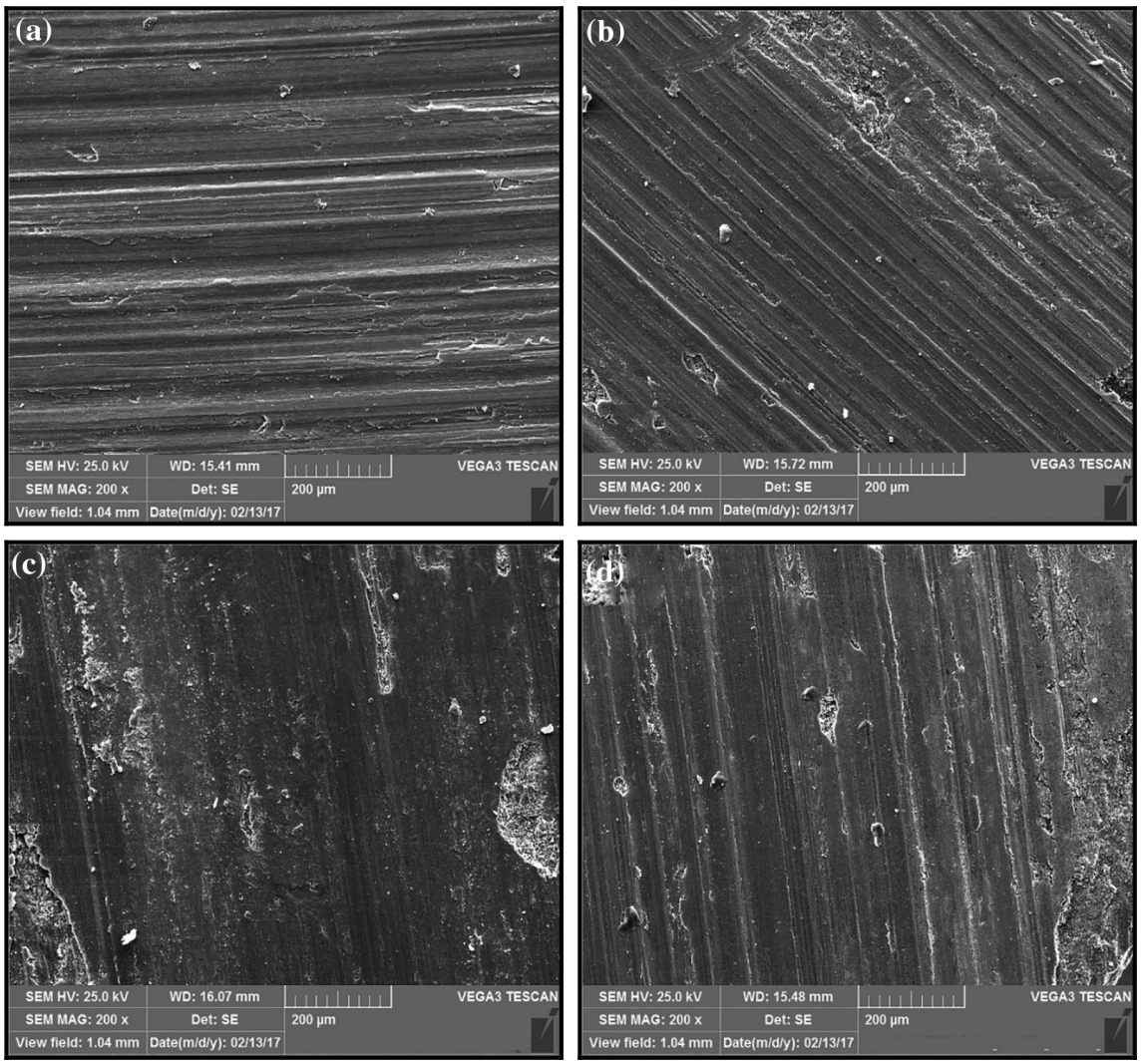

Fig. 10 SEM micrographs of worn surface of **a** AA5083 alloy, **b** AA5083–B_4C, **c** AA5083–SiC, **d** AA5083–TiC surface composites

along the sides of the grooves. Asperities are formed during the process of sliding surfaces in contact inducing the frictional heat which softens the matrix alloy and more materials are removed from pin samples thus forming wear debris. Subsequently wear debris, pin sample and counter disk further lead to the three body abrasive wear mechanism [9]. Figure 10b–d shows the SEM micrograph of the worn surface of AA5083 surface composites reinforced with various particulates. It is evident from the SEM micrographs that sign of plastic deformation is little. This can be attributed to the presence of particulates restricting the flow of the material during the frictional sliding wear. As a result of this, the worn surface shows both the abrasive and delamination wear mechanism. This can be due to the higher hardness, refined grain and excellent bonding of particle with the matrix which can lower the plastic deformation. The worn surface of AA5083 surface composites indicates fine grooves and small-sized pits or crater which are clearly visible in the SEM micrograph and followed by less debris. The presence of oxide layer on worn surfaces can be attributed to the mild wear, as sliding wear proceeds interaction between pin and counterface increases the temperature. Therefore, a protective oxide film is formed on the surface and this film can render the severe wear to mild wear. The formation of mechanically mixed layer (MML) of aluminum oxide/iron oxide resulting from the frictional heat of contact surface induces high temperature during sliding wear. A similar occurrence of MML in metal matrix composite was reported by several researchers [9, 10]. Figure 11 shows the SEM micrograph of wear debris obtained from AA5083 to AA5083 surface composites reinforced with different particulates. The wear debris of aluminum matrix in Fig. 11a shows the large plate-like structure of irregular shapes of different dimensions indicating severe plastic deformation. The morphology of wear debris suggests that the material removal is

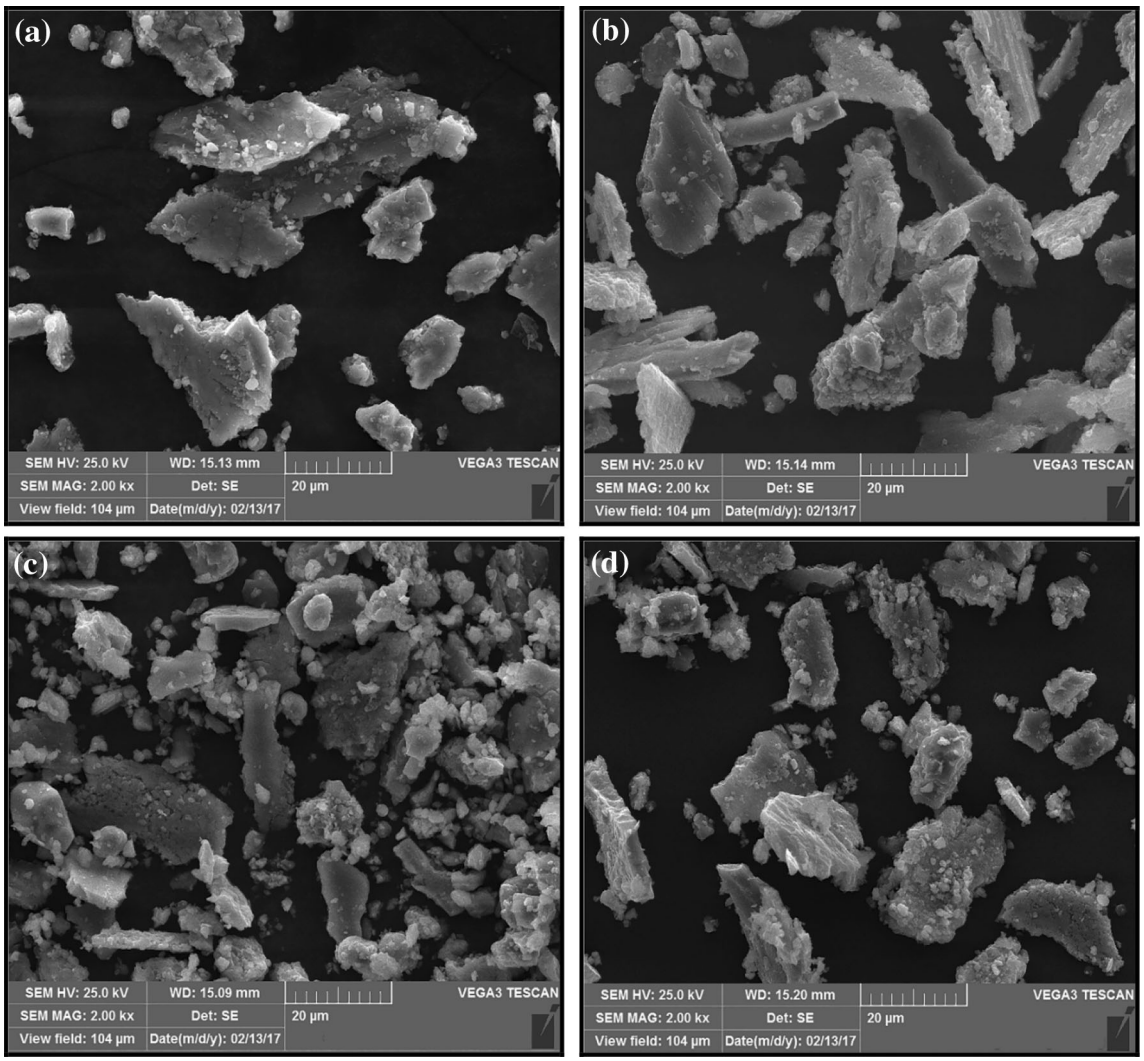

Fig. 11 SEM micrographs of wear debris of **a** AA5083 alloy, **b** AA5083–B_4C, **c** AA5083–SiC, **d** AA5083–TiC surface composites

dominated by abrasive and delaminated wear [15]. The significant change in morphology of the wear debris of AA5083 surface composite is shown in Fig. 11b–d, which reveals smaller flake like debris and fine particles compared to base alloy. This attributes to increase in hardness of composite due to embedded particulates, that reduces softening of composite leading to lesser plastic deformation.

4 Conclusion

The reinforcement of different particulates was successfully incorporated into the aluminum matrix so as to fabricate aluminum surface layered composite via friction stir processing. The microstructure, hardness, tensile properties, and wear behavior of the composite were evaluated.

- The metallographic evaluation revealed that the dense formation of particulates from retreating side to advancing side, distribution of particulates at the stir zone, and particle free region were observed.
- Multi pass FSP refined the grain structure of surface composites and pinning effect of particles retarded the grain growth.
- The highest microhardness was observed for AA5083–B_4C composite when compared to the other composites and base alloy.
- An increase in the tensile strength was observed for surface composite. This attributed to the addition of particulates acting as obstacles for movement of dislocations.
- The fracture surface of TiC and SiC reinforced composites prepared by FSP showed smaller voids and dimples compared to base alloy whereas, B_4C reinforced surface composite displayed distribution of

smaller dimples and tear ridges confirming the bimodal distribution of fracture.

- The wear rate considerably showed decreasing trend for all the surface composites samples when compared to the base alloy, because of uniform dispersion of particulates and grain refinement.

Acknowledgements The author (Vikram Kumar S. Jain), would like to thank Department of Science & Technology, Govt. of India for sponsoring him to pursue Ph.D. under INSPIRE Fellowship (DST/INSPIRE Fellowship/2015/IF150488).

References

1. Shorowordi K M, Laoui T, Haseeb A S M A, Celis J P, and Froyen L, *J Mater Process Technol* **142** (2003) 738.
2. Amouri K, Kazemi S, Momeni A, and Kazazi M, *Mater Sci Eng A* **674** (2016) 569.
3. Erdemir F, Canakci A, and Varol T, *Trans Nonferrous Met Soc China* **25** (2015) 3569.
4. Kallip K, Babu N K, Alogab K A, Kollo L, Maeder X, Arroyo Y, and Leparoux M, *J Alloys Compd* **714** (2017) 133.
5. Khodabakhshi F, and Simchi A, *Mater Des* **130** (2017) 26.
6. Li Y, Lin Li Q, Li D, Liu W, and Gang Shu G, *Trans Nonferrous Met Soc China* **26** (2016) 2304.
7. Mishra RS, Ma Z Y, and Charit I, *Mater Sci Eng A* **341** (2003) 307.
8. Chen Z, Li J, Borbely A, Ji G, Zhong S Y, Wu Y, Wang M L, and Wang H W, *Mater Des* **88** (2015) 999.
9. Dinaharan I, Nelson R, Vijay S J, and Akinlabi E T, *Mater Charact* **118** (2016) 149.
10. Khodabakhshi F, Simchi A, and Kokabi A H, *Surf Coatings Technol* **309** (2017) 114.
11. Narimani M, Lotfi F, and Sadeghian Z, *Surf Coatings Technol* **285** (2016) 1.
12. Kumar PA, Yadav D, Chandra S P, and Kailas S V, *Mater Des* **113** (2017) 99.
13. Mahmoud E R I, Ikeuchi K, and Takahashi M, *Sci Technol Weld Join* **13** (2008) 607.
14. Shafiei-Zarghani A, Kashani-Bozorg S F, and Zarei-Hanzaki A, *Mater Sci Eng A* **500** (2009) 84.
15. Rejil C M, Dinaharan I, Vijay S J, and Murugan N, *Mater Sci Eng A* **552** (2012) 336.
16. Soleymani S, Abdollah-zadeh A, and Alidokht S A, *Wear* **278** (2012) 41.
17. Yuvaraj N, Aravindan S, and Vipin, *J Mater Res Technol* **4** (2014) 398.
18. Roy T K, Subramanian C, Suri A K, *Ceram Int* **32** (2006) 227.
19. Mazaheri Y, Meratian M, Emadi R, and Najarian A R, *Mater Sci Eng A* **560** (2013) 278.
20. Liew K M, Kai M F, and Zhang L W, *Compos Struct* **160** (2017) 81.
21. Yuvaraj N, Aravindan S, and Vipin, *Trans Indian Inst Met* **70** (2017) 1111.
22. Bauri R, Yadav D, and Suhas G, *Mater Sci Eng A* **528** (2011) 4732.
23. Dong J, Zhang M, Xie X, and Thompson R G, *Mater Sci Eng A* **328** (2002) 8.
24. Ishida K, *J Alloys Compd* **235** (1996) 244.
25. Ping D H, Gu Y F, Cui C Y, and Harada H, *Mater Sci Eng A* **456** (2007) 99.
26. Rohatgi P K, Yarandi F M, Liu Y, and Asthana R, *Mater Sci Eng A* **147** (1991) 1.
27. Seniw M E, Conley J G, and Fine M E, *Mater Sci Eng A* **285** (2000) 43.
28. Sasikumar R, and Kumar M, *Acta Metall Mater* **39** (1991) 2503.
29. Dinaharan I, Sathiskumar R, and Murugan N, *J Mater Res Technol* **5** (2016) 302.
30. Yuvaraj N, Aravindan S, and Vipin, *Surf Coatings Technol* **309** (2017) 309.
31. Ashjari M, Mostafapour Asl A, and Rouhi S, *Mater Sci Eng A* **645** (2015) 40.
32. Khodabakhshi F, Gerlich A P, and Svec P, *Mater Sci Eng A* **698** (2017) 313.
33. Narimani M, Lotfi B, and Sadeghian Z, *Mater Sci Eng A* **673** (2016) 436.
34. Zhang Z, and Chen D L, *Mater Sci Eng A* **483** (2008) 148.
35. Zhang Z, Yang R, Guo Y, Chen G, Lei Y, Cheng Y, and Yue Y, *Mater Sci Eng A* **689** (2017) 411.